Structure
Article

The Structure of the C-Terminal KH Domains of KSRP Reveals a Noncanonical Motif Important for mRNA Degradation

María Flor García-Mayoral,[1,5] David Hollingworth,[1,5] Laura Masino,[1] Irene Díaz-Moreno,[1] Geoff Kelly,[2] Roberto Gherzi,[3] Chu-Fang Chou,[4] Ching-Yi Chen,[4] and Andres Ramos[1,*]
[1] MRC National Institute for Medical Research, The Ridgeway, Mill Hill, London NW7 1AA, UK
[2] MRC Biomolecular NMR Centre, The Ridgeway, Mill Hill, London NW7 1AA, UK
[3] Gene Expression Regulation Laboratory, Istituto Nazionale per la Ricerca sul Cancro, 16132 Genova, Italy
[4] Department of Biochemistry & Molecular Genetics, University of Alabama at Birmingham, Birmingham, AL 35294, USA
[5] These authors contributed equally to the work.
*Correspondence: aramos@nimr.mrc.ac.uk
DOI 10.1016/j.str.2007.03.006

SUMMARY

The AU-rich element (ARE) RNA-binding protein KSRP (K-homology splicing regulator protein) contains four KH domains and promotes the degradation of specific mRNAs that encode proteins with functions in cellular proliferation and inflammatory response. The fourth KH domain (KH4) is essential for mRNA recognition and decay but requires the third KH domain (KH3) for its function. We show that KH3 and KH4 behave as independent binding modules and can interact with different regions of the AU-rich RNA targets of KSRP. This provides KSRP with the structural flexibility needed to recognize a set of different targets in the context of their 3′UTR structural settings. Surprisingly, we find that KH4 binds to its target AREs with lower affinity than KH3 and that KSRP's mRNA binding, and mRNA degradation activities are closely associated with a conserved structural element of KH4.

INTRODUCTION

Adenosine-uridine-rich element (ARE)-mediated mRNA decay (AMD) provides the organism with an important tool for gene regulation and has been related to cellular proliferation, immune response, and cardiovascular toning. Indeed, impaired AMD results in abnormal cell proliferation and angiogenesis, leading to cancer (Audic and Hartley, 2004). AMD malfunction has also been linked to inflammatory diseases such as Crohn-like inflammatory bowel disease and inflammatory arthritis (Kontoyannis et al., 1999).

AMD regulates the concentration of mRNAs that contain AREs within their 3′ untranslated regions (3′UTRs) by promoting their degradation. Among the many mRNAs known to be regulated by AMD are those encoding tumor necrosis factor α (TNFα), IL-10, cJUN, cFOS, and cyclins D1 and D3 (Bakheet et al., 2006). AMD is mediated by the binding of regulatory proteins, the ARE-binding proteins (ARE-BPs), to the mRNA. However, not all ARE-BPs destabilize mRNAs; the members of the Hu family, which act as antagonists to other decay-promoting ARE-BPs, have a stabilizing effect (Barreau et al., 2006).

Information on the RNA targets of several ARE-BPs is available and, in two cases, structural information on the interaction has also been obtained (Hudson et al., 2004; Wang and Tanaka Hall, 2001). This information reveals a link between the functions of these proteins and the level of specificity shown for their target mRNAs. The TIS11d protein family promotes the decay of a small subset of mRNAs (for example, TNFα), and TIS11d itself has been reported to bind specifically to the UUAUUUAUU sequence with two zinc finger motifs (Hudson et al., 2004). Conversely, HuD, a member of the Hu family, uses two RRM domains to recognize U-rich sequences with little sequence specificity (Wang and Tanaka Hall, 2001). Most ARE-BPs, have a limited but important target specificity (Barreau et al., 2006) that place them in between these two extremes and fulfill a partially redundant role in mRNA decay. However, defining the elements of target specificity is difficult, partly because of the functional redundancy of ARE-BPs and partly because of the heterogeneous length and structure of the ARE targets themselves. The most commonly used classification catalogs AREs in three groups depending on the presence and on the arrangement of AUUUA motifs inserted within the U-rich sequences. A further level of complexity derives from the poorly defined ARE boundaries and the lack of information on the secondary structure of the ARE-containing mRNAs.

K-homology splicing regulator protein/fuse binding protein 2 (KSRP/FBP2) is an important ARE-BP that is known to interact with several different AREs. The central part of the protein is organized in four K-homology domains (Figure 1). A study on the functional mechanisms of KSRP has provided an insight into its role in AMD. KSRP recruits the exosome and deadenylation factors to the mRNAs,

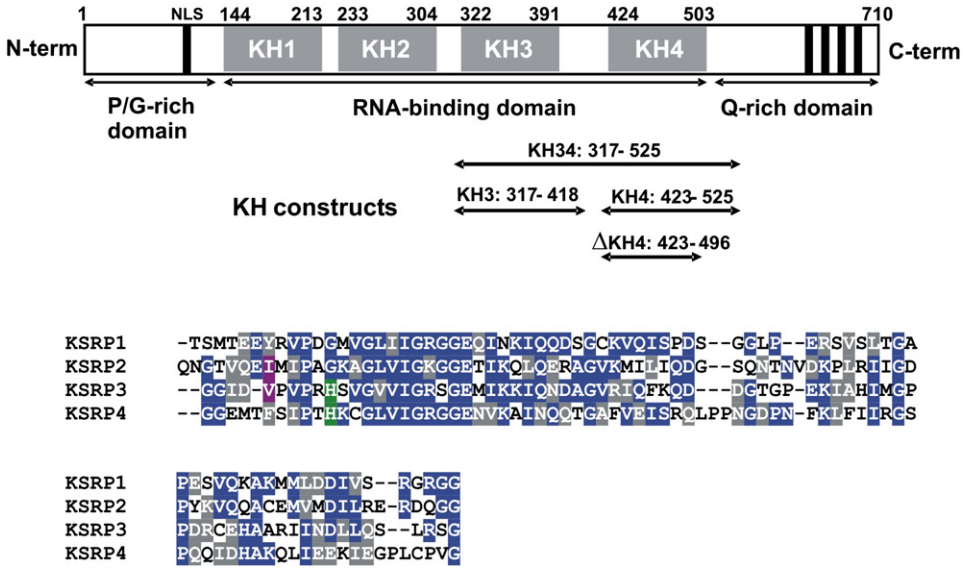

Figure 1. KSRP Protein

Domain organization of KSRP with constructs used in this study (top) and sequence alignment of the four KSRP KH domains (bottom). Blue and green indicate strictly conserved residues in two or more domains; gray and purple, conservative substitutions of hydrophobic and polar residues.

leading first to polyA shortening and then to 3′-to-5′ exonucleolytic digestion of the mRNA targets (Gherzi et al., 2004). More recently, two papers reported phopshorylation-mediated mechanisms that link the functional and transient shut off of KSRP-mediated mRNA decay to extracellular processes (Gherzi et al., 2006; Briata et al., 2005). The information available on KSRP makes this protein an efficient model system to study the regulation of mRNA degradation by the AREs at the molecular level.

Using qualitative crosslinking and mRNA decay assays, Gherzi et al. have shown that the third (KH3) and fourth (KH4) domains of KSRP are necessary for mRNA degradation (Gherzi et al., 2004). However, KH3 and KH4 play different roles. KH4 is essential for mRNA decay and ARE recognition, and its deletion results in the complete loss of these activities. Deletion of KH3 instead does not have such a severe effect on ARE recognition. Nevertheless, KH4 by itself is not sufficient for recognition as deletion of KH1-3 leads to impaired interaction and decay. Only when KH4 is accompanied by KH3, is the protein capable of ARE recognition and mRNA decay. Although the role of KH1 and KH2 in RNA binding and ARE recognition needs further analysis, this study focuses on the two KH domains that appear to be most important for mRNA decay, KH3 and KH4. In particular, we wish to elucidate the role of KH4 in the recognition of different AREs and in the subsequent degradation of the corresponding mRNAs.

Using NMR, CD, and mRNA degradation assays, we have analyzed the elements that contribute to KH domain-RNA interactions and mRNA degradation. We have studied the structure and dynamics of KH3 and KH4 and the relationship between the two domains. We have dissected their RNA-binding characteristics and demonstrated that KH3 plays a direct and important role in the interaction with the RNA. We have also shown that the functional relevance of KH4 is associated with a novel structural element within the domain that tunes mRNA recognition.

RESULTS

In order to investigate the contributions of KH3 and KH4 to KSRP-mediated ARE binding and mRNA degradation, we have solved the structure of the two domains and analyzed their relationship and RNA-binding properties. We want to understand how the protein capitalizes on its multidomain structure to bind different targets in the context of large, structured, RNA 3′UTRs and how this interaction is regulated.

Analysis of the Structure and Motions of KH3 and KH4 Domains

As a first step, we have analyzed the structure of the third and fourth KH domains of KSRP separately and as a unit. The secondary structure elements are well defined in both KH3 and KH4 structures, including the novel fourth strand of KH4, and the analysis of the ϕ and φ angles indicates that all assigned residues lie in the most favored regions of the Ramachandran plot (Table 1). The few (~1%) residues in the disallowed regions belong to the invariant and variable loops for which no assignment and structural constraints are available.

KH3 folds as a ~70-residue canonical eukaryotic KH domain of topology $\beta\alpha\alpha\beta\beta\alpha$ (Gly 324-Arg 394) (Figure 2A). The N- and C-terminal ends of the construct are unstructured and flexible. The highly exposed invariant GXXG loop, which is often not observed in solution (Musco et al., 1997), is indeed only partially visible in the free protein

Table 1. Structural Constraints and Statistics of Water-Refined KSRP KH3 and KH4 Domains

	KH3	KH4
Distance restraints	2037	2340
Intraresidual	832	852
Sequential ($\|i - j\| = 1$)	401	517
Medium range ($1 < \|i - j\| < 4$)	241	291
Long range ($\|i - j\| > 4$)	563	680
Experimental ϕ constraints	27	47
TALOS ϕ and φ constraints	52	0
Hydrogen-bond constraints	23	25
Energy Statistics (20 Conformers)		
Mean total energy (kcal/mol)	−3324 ± 10	−3462 ± 15
NOE violations > 0.3Å	0.2 ± 0.4	0.1 ± 0.3
Mean NOE energy (kcal/mol)	28 ± 1	34 ± 1
Rmsd from Idealized Covalent Geometry		
Bonds (Å)	0.016 ± 0.001	0.017 ± 0.001
Angles (°)	0.26 ± 0.07	0.3 ± 0.1
Ramachandran Plot Analysis		
Most favored regions (%)	93.2	89.7
Additional allowed regions (%)	5.7	9.5
Generously allowed regions (%)	0.2	0.4
Disallowed regions (%)	1.0	0.4
Rmsd from the Mean Structure (Å)		
Whole structured domain[a]		
Backbone atoms	0.86 ± 0.21	0.67 ± 0.12
Heavy atoms	1.66 ± 0.25	1.32 ± 0.17
Secondary structure[b]		
Backbone atoms	0.51 ± 0.10	0.53 ± 0.09
Heavy atoms	1.25 ± 0.16	1.10 ± 0.13

[a] KH3 whole structured domain: 324–394. KH4 whole structured domain: 425–503.
[b] KH3 secondary structure: 324–338, 343–359, and 367–393. KH4 secondary structure: 425–440, 445–461, and 471–503.

(data not shown). A second variable seven-residue loop between β_2 and β_3 shows lower-than-average heteronuclear NOE values (<0.70), indicating high frequency (ns to ps) motions (Figure S2 and Table S2 available with this article online).

The structure of KH4 (Gly 425-Gly 503) (Figure 2A) shows a few significant differences with respect to KH3. KH4 has a shorter C-terminal helix, a longer variable loop, and, most importantly, an additional C-terminal strand, β_4 (Figure 2B). The backbone dynamics of KH3 and KH4 are similar, although shorter than average T_2 values, and large T_1/T_2 ratios are measured for residues in and around the invariant GXXG loop (V337, I338, G339, G342, M344, and I345) for KH3 but not for KH4 (Figure 3). These data suggest that, in KH3, these residues can undergo conformational rearrangement in the μs-ms time scale, a behavior often associated with biologically relevant conformational motions. The GXXG loop of KH domains is crucial for nucleic acid binding, and these motions may therefore be related to the higher RNA-binding activity of KH3.

Despite these differences, KH3 and KH4 have a globally similar structure. A structural alignment between KH3 (Gly 324-Arg 394) and KH4 (Gly 425-Gly 503) using the DALI (Holm and Sander, 1993) database server has returned a z score value of 9.7, with an rmsd value of 2.1 Å for the aligned residues. This value is not very different from the one obtained by searching the PDB for similar structures. Comparison with the KH3 and KH4 domains of another member of the FBP family, the Far upstream element (FUSE) binding protein 1 (1j4w) (Braddock et al., 2002), returned z scores of 11.1 and 9.5, respectively, while comparison with the KH3 domain of Nova-1 (1dt4) has returned a z score of 10.1 and 9.1 for KH3 and KH4. Importantly, DALI consistently excluded the fourth strand of KH4 from any alignment. Thus, both KH3 and KH4 are classical KH domains, if we exclude the novel strand observed in KH4.

KH4 β_4 is a 4 residue (L499, C500, P501, and V502) element. The strand is at a significant angle with respect to the main β sheet and crosses with strand β_1. Only one hydrogen bond is formed between the backbone atoms of V502 (HN) and T428 (O) (Figure 2C). However, the side chains of residues L499, C500, P501, and V502 make contacts with residues T428, F429, S430, and I431 in the β_1 strand, anchoring β_4 to the domain.

Preliminary to a more in-depth structural and functional analysis of β_4, we examined its conservation in the KSRP family. The alignment of the sequences of the KH4 domain in rat (*Rattus norvegicus*), chicken (*Gallus gallus*), and frog (*Xenopus laevis*) reveals that the residues in β_4 are well conserved (Figure 2D). This observation strongly suggests that the additional strand is present in those proteins and might be performing a common function. In contrast, the remaining KH domains of KSRP do not have conserved hydrophobic amino acids C-terminal to the standard KH fold (Figure 2E). The role of this strand is therefore linked to a specific function of KH4. Comparison of NOESY spectra of the KH3, KH4, and KH34 constructs confirm that the structures of the isolated domains do not change significantly in the longer construct.

The Third and Fourth Domains of KSRP Are Independent Structural Units Joined by a Flexible Linker

The role that the KH3 and KH4 domains play in the identification of target RNAs depends on their affinity and specificity for the RNA molecules but may also rely on interdomain interactions. KSRP target sequences, albeit probably unfolded, are embedded within the structured 3′UTR of the mRNAs. A preformed protein-protein interaction may be an important factor in limiting accessibility to the RNA targets.

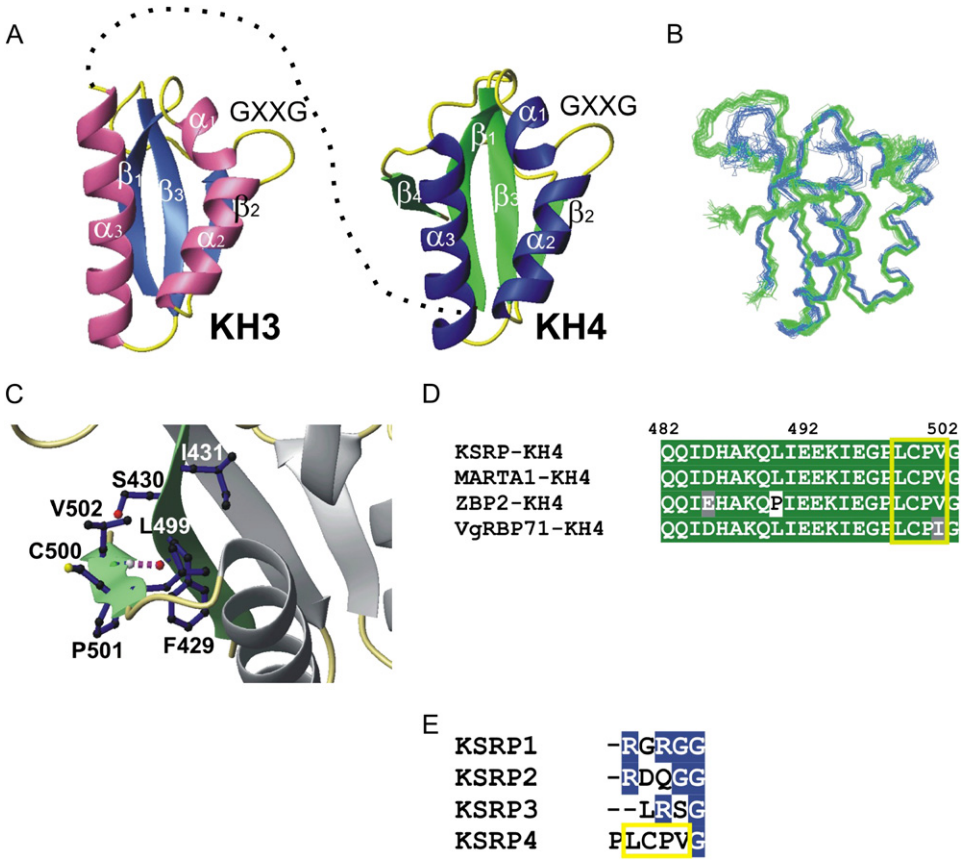

Figure 2. Structures of KH3 and KH4

(A) Ribbon model of representative conformers of the solution structure families of the KH3 (left) and KH4 (right) KSRP domains (MolMol).

(B) Superposition of KH3 (blue) and KH4 (green) 20 lowest energy conformers. The domains have been rotated 90° to visualize more clearly the structural differences.

(C) Close up of the side-chain interactions between the β_4 and β_1 strands of KH4. The hydrogen bond between T428 O and V502 HN is indicated with a magenta-dashed cylinder.

(D) Sequence alignment of the C terminus of the KH4 domains in the KSRP/FBP2 family. The rat (*Rattus norvegicus*, MARTA1), chicken (*Gallus gallus*, ZBP2), and frog (*Xenopus laevis*, VgRBP71) homologs are aligned with human KSRP. Residues in gray indicate conservative mutations. A yellow box defines the boundaries of β_4.

(E) Blow up section of the alignment in Figure 1. The residues forming β_4 in KH4 are not conserved in KH1, KH2, and KH3.

To directly test specific interactions between domains, we have compared fingerprint NMR spectra for the domains in isolation and within a two-domain construct. Superimposition of ^{15}N-HSQC spectra of KH3, KH4, and KH34 (Figure 4A) shows that chemical shift differences are small (±0.02 ppm) and evenly distributed along the sequence (Figure S1) and that resonances from amide groups in the linker are in the random-coil region. This indicates that KH3 and KH4 are not interacting specifically with each other and are joined by a flexible linker.

The analysis of the NMR relaxation properties of the domains supports this conclusion. We recorded NMR relaxation experiments (^{15}N T_1 and T_2, and ^{15}N(^{1}H) NOE) on ^{15}N-labeled samples of KH3, KH4, and KH34 and estimated a global rotational correlation time (τ_c) for the two domains. The τ_c values obtained (KH3, 6.36 ns, and KH4, 6.85 ns) (Table S1) are in good agreement with values reported for other monomeric KH domains (Baber et al., 1999; Musco et al., 1997). Importantly, a small difference is observed between the τ_c of the two domains, consistent with the slightly larger size of KH4. This difference is conserved when the two domains are part of the same construct (τ_c of KH(3)4 and KH3(4) are, respectively, 8.13 and 8.51 ns) (Table S1), indicating that the rotational behavior of the two domains does not change when they are covalently linked. The minor increase in the τ_c value, visible for both domains in KH34, is expected: Brownian dynamic simulations have shown that addition of a second domain tethered to a flexible linker has a non-negligible effect on the correlation time (Bernadó et al., 2004).

In order to validate the NMR relaxation data, we examined the reorientation of the molecule in aligned media. We analyzed the differences between the alignment tensors of the two separated domains in $C_{12}E_5$ magnetically ordered

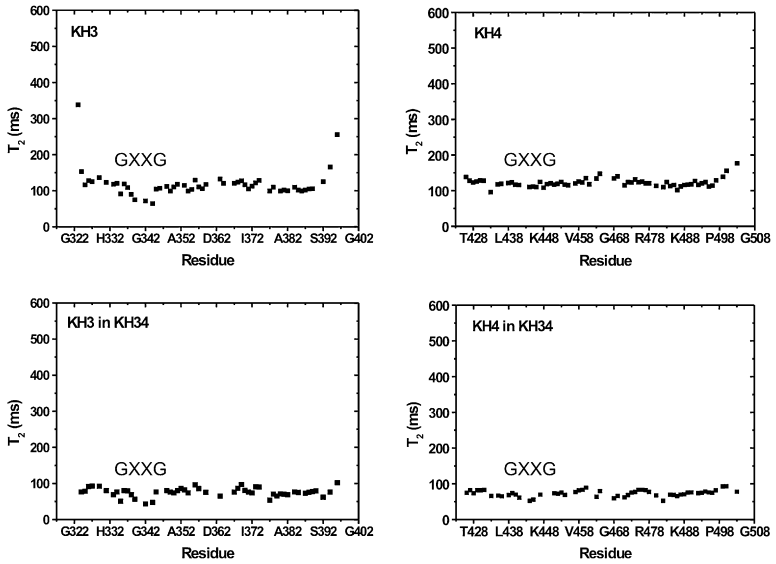

Figure 3. KH3 and KH4 Internal Motions
^{15}N amide T_2 measurements for isolated KH3 and KH4 at 600 MHz ^{1}H frequency (top) are compared with analogous measurements recorded on the two-domain construct (bottom). The T_1 and heteronuclear NOE values are reported in the Figure S2 and Table S2.

liquid-crystalline phases (Rückert and Otting, 2000) and compared them with the difference in the two-domain construct. Alignment tensor parameters for the domains have been estimated in the absence of a priori structural information from the experimental histogram of measured RDCs (Clore et al., 1998) and, as expected (Braddock et al., 2001), are very similar. However, a difference exists in the rhombicity of the domains (R ~0.4 for KH3 versus R ~0.3 for KH4) (Table S1). More importantly, a significant difference also exists in the two-domain construct (similar to that of the isolated domains) (Table S1), providing further evidence for an independent rotation of the protein domains.

Finally, we analyzed the thermal stability of KH3, KH4, and KH34 by CD (Figure 4B). Changes in the stability of the two domains may be attributed to weak interdomain contacts (Masino et al., 2000). Two very similar (62°C ± 1°C and 61°C ± 1°C) transition midpoints (T_m) were observed for the individual KH3 and KH4 domains, while only one transition (with T_m = 62°C ± 1°C) could be resolved in KH34. This suggests that addition of the neighboring domain does not change significantly the stability of either KH3 or KH4. This result was confirmed by recording ^{15}N-HSQC NMR spectra in the 27°C –69°C temperature range for KH3, KH4, and KH34 and by monitoring the unfolding of the two domains separately and together (data not shown). Our data suggest that the KH3 and KH4 domains of KH34 are joined by a flexible linker and do not make specific contacts nor stabilize each other.

RNA-Binding Properties of KH3 and KH4

To understand how the KSRP-RNA interaction may be regulated, we assessed the affinity of KH3 and KH4 for their RNA target and explored if the specificity of each domain for a cognate sequence could drive recognition. We used two different techniques, NMR and CD, to obtain quantitative data over a wide range of affinities. Preliminary binding assays by NMR indicate that both KH3 and KH4 interact with the TNF RNA using the canonical RNA binding surface of KH domains (α_1, α_2, β_2, GXXG loop) (Figure 5B) (Lewis et al., 2000). This observation (with small variations) holds for KH3 and KH4 in isolation and within KH34, for all tested RNAs, and defines RNA binding by these KH domains of KSRP as a ''classical'' KH-RNA interaction.

We used RNA oligonucleotides derived from TNFα ARE, the best studied RNA target of KSRP, to dissect the RNA-binding properties of the KH3, KH4, and KH34 constructs (Figure 6). The core TNFα ARE sequence is a 25-nucleotide-long sequence that contains two repeats of the UAUUUAUUAUUU element. The binding site of a single KH domain is known to vary between 4 and 6 nucleotides (Musunuru and Darnell, 2004), and a 12-nucleotide RNA of sequence UAUUUAUUAUUU (Figure 6) contains all possible single KH-binding sites in TNF_α ARE core. Binding of KH3 and KH4 to this RNA should reflect their ability to bind to the TNF_α ARE, regardless of their sequence specificity. Our CD and NMR data show that the affinity of the two domains for the RNA is in the low micromolar range, with KH3 binding approximately four times tighter than KH4 (Table 2). It is therefore unlikely that the importance of the role of KH4 in mRNA decay derives from a strong binding affinity. Next, we investigated whether either KH3 or KH4 show a strong preference for a specific site within the TNF_α ARE, a site that could act as the main determinant for KSRP positioning on the RNA. The sequence of the TNF_α ARE is a run of two or three Us separated by single As (Figure 6). Sequences that occur many times within the TNF_α ARE (e.g., UAUU, six times; UAU, seven times) would not reduce significantly the number of positions each domain can assume on the long RNA. Instead, the AUUUA and AUUA sequences are present in a smaller number of copies (four and two, respectively). Recognition of these sequences could be important to position a domain on the TNF_α ARE, especially if the choice of site is further limited by the concurrent recognition of another site

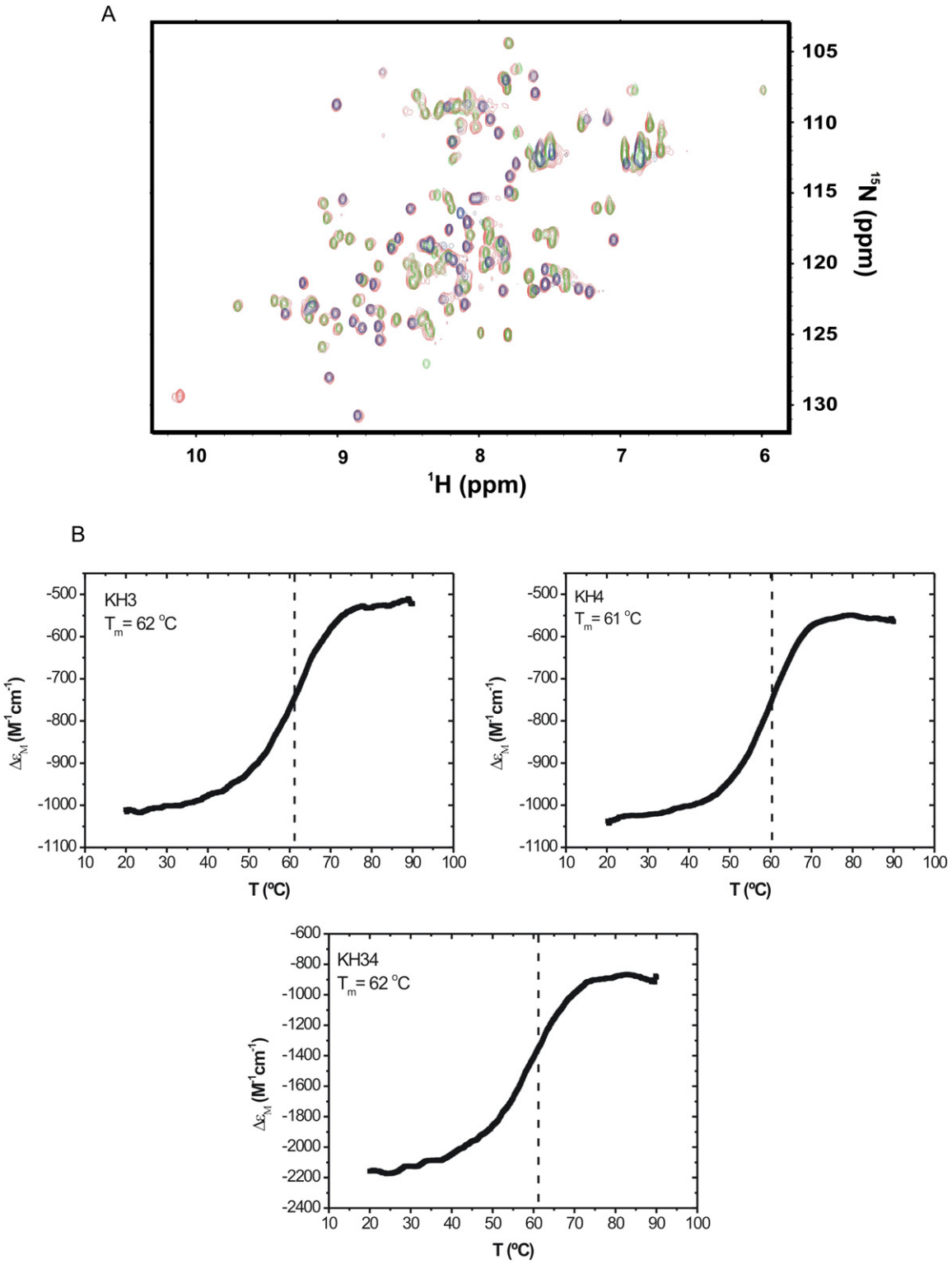

Figure 4. Relationship between KH3 and KH4

(A) Superimposition of ^{15}N-HSQC spectra of KH3 (blue), KH4 (green), and KH34 (red) at 27°C and pH 7.4. The spectra of the two domains do not change in the two-domain construct, indicating that the structure is conserved and no stable interaction is taking place. Plots with the (very small) chemical shift differences measured in the overlapped spectra are shown in Figure S1.

(B) 220 nm CD signal of KH3, KH4, and KH34 as a function of temperature during the thermal denaturation of the domains. All unfolding transitions have a similar midpoint indicated by a dashed line.

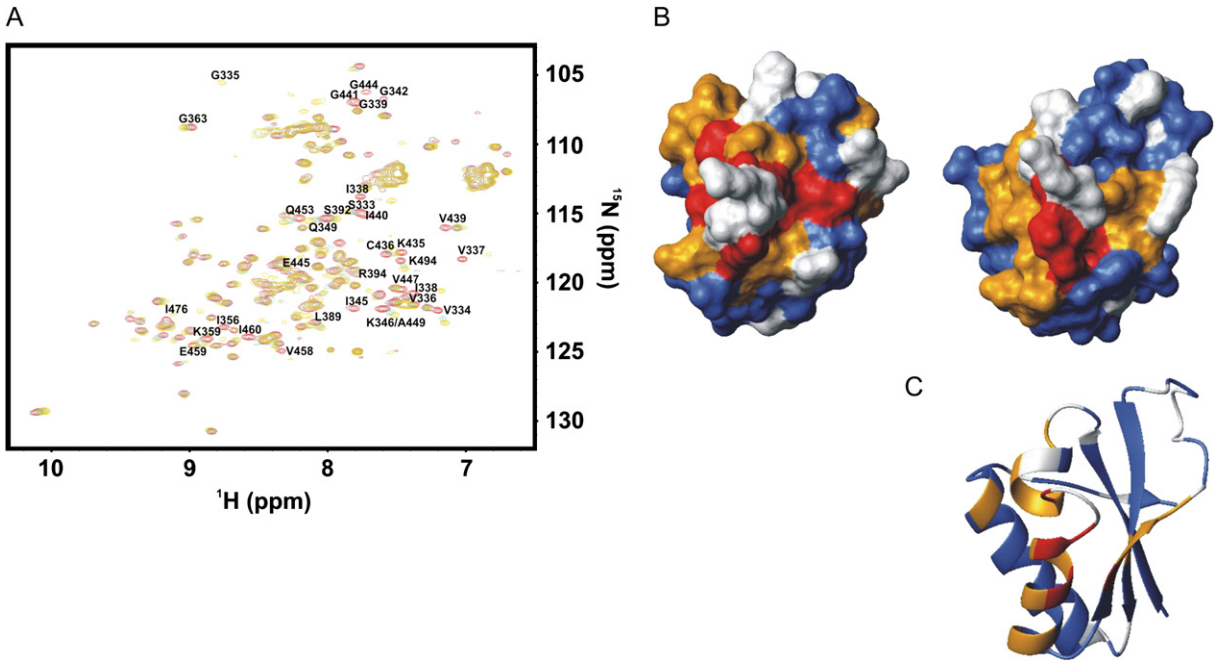

Figure 5. RNA Binding of KH3, KH4, and KH34 with 12-mer RNA

(A) Superimposition of a series of ^{15}N-HSQC spectra recorded during a titration of KH34 with increasing amounts of UAUUUAUUAUUU RNA. A subset of resonances of the free protein (red) shift when 0.3 (cyan) and 1 (yellow) equivalents of RNA are added. At 1:1 ratio, the protein is completely saturated. Several representative resonances are labeled.

(B) Averaged ^{1}H and ^{15}N chemical-shift changes of KH3 (left) and KH4 (right) upon interaction with the 12-mer RNA oligonucleotide are mapped on the domain surfaces (MolMol). Residues are colored according to the magnitude of their average chemical-shift perturbations at 1:4 protein/RNA ratio: $\Delta\delta_{aver} > 0.2$, red; $0.2 > \Delta\delta_{aver} > 0.05$, orange; $\Delta\delta_{aver} < 0.05$, blue. Proline, nonobserved, and overlapped residues are depicted in white.

(C) Ribbon display of the chemical-shift perturbation mapping of KH4 in the same orientation and color code as (B), highlighting which secondary structure elements are involved in the interaction. Residues in the additional strand β_4 do not shift significantly upon RNA binding. Both KH3 and KH4 bind to RNA with the canonical KH nucleic acid-binding groove, common to all the structures/studies of KH-RNA/DNA complexes.

by a second domain of KSRP. Therefore, we tested the binding affinity of KH3 and KH4 for the UAUUUA and UAUUAU RNAs. NMR data show that both KH3 and KH4 bind in the submillimolar range to either RNA, with KH3 binding 2- to 3-fold tighter than KH4 (Table 2), indicating that neither domain is likely to drive the KSRP-RNA interaction by positioning itself on a unique RNA sequence. CD titrations showed that binding of KH34 to the RNA 12-mer is tighter than the binding of the single domain constructs (Table 2). Consistently, at NMR concentrations, this binding is stoichiometric, and saturation is reached at 1:1 protein:RNA ratio. Tighter binding is caused by the involvement of both domains in the interaction: selective changes in the positions of NMR peaks are observed for resonances of both KH3 and KH4 within KH34 (Figure 5A).

Summarizing, specificity of the isolated KH3 and KH4 domains for a short RNA sequence is unlikely to alone position KSRP on its TNF$_\alpha$ ARE target. Indeed, some of the known ARE targets of KSRP do not contain the AUUUA pentamer but other AU-rich sequences. The relatively weak binding of KH4 suggests that this domain is not a simple RNA-binding platform but performs a role linked to its unique and conserved structural features.

KH4 β_4 Is an Essential Structural Element Important in RNA Binding and mRNA Decay

β_4 represents a novel extension of the KH domain and is essential for the stability of KH4. The NMR resonances of β_4 disappear at the same temperature as the resonances of the core of the domain in thermal unfolding experiments. Further, the ΔKH4 construct, a shorter version of KH4 that does not include β_4, is unstable at 27°C, but not at 15°C (Figure S3). Unfortunately, as this mutant is largely unfolded at 37°C, it is not possible to establish the functional relevance of KH4 by completely removing the strand.

We therefore attempted a more subtle tuning of the interaction between β_4 and the domain, by mutating Leu 499 to Ala (Figure 2C), thereby removing several hydrophobic contacts between the strand and the main hydrophobic core. In contrast with the deletion mutant, the KH4L499A mutant provides high quality HSQC spectra in the range of temperatures tested (Figure 7A). The good dispersion of the resonances and the limited changes in the spectra indicate that the mutant conserves its KH fold. However, chemical-shift differences between wild-type and mutant extend to a large section of the β sheet, indicating a subtle effect on the protein structure not limited

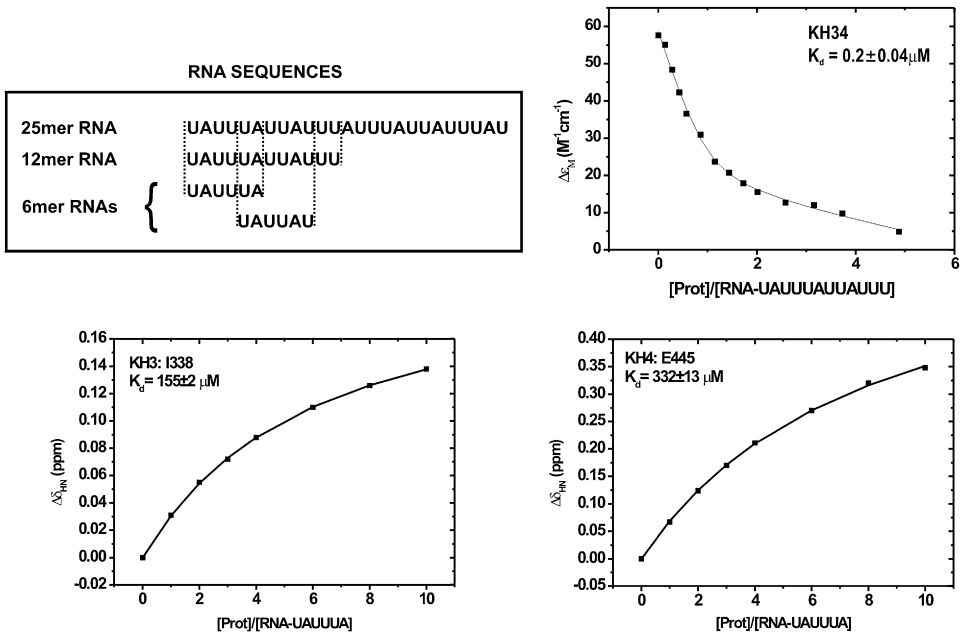

Figure 6. Comparison of KH3, KH4, and KH34 Affinities for a Target RNA

Top left, RNA sequences tested in this study. Top right, changes in the CD signal in the 255–265 nm region of the 12-mer RNA oligonucleotide spectrum during a titration with KH34. Bottom, plots of amide chemical-shift changes measured during NMR titrations of KH3 (left) and KH4 (right) displayed as function of the protein/RNA ratio. One representative residue is shown for KH3 (I338, left) and KH4 (E445, right). Dissociation constants are also shown.

to the β_4 region (Figure S4A). This is confirmed by the widespread increase in high-frequency motions observed upon mutation (Figure S4B). Using CD, we have established that the unfolding T_m for the mutant is 50°C ± 1°C, ~10°C lower than for the wild-type (Figure 7B), indicating that >85% of the protein is folded at 37°C. The mutant is amenable to functional studies.

To establish the effect of this single-point mutation on mRNA decay, mutant and wild-type constructs were used in a comparative mRNA degradation assay. We coexpressed FLAG-tagged full-length KSRP or the Leu to Ala mutant, KSRPL499A, with a globin mRNA reporter containing the ARE of GM-CSF (GB-ARE^{GMCSF}) that includes a string of AUUUA elements, under the control of a tetracycline-regulatory promoter, in an established HT 1080-TO (Tet-Off) cell line, and examined the decay of GB-ARE^{GMCSF} mRNA in a transcriptional pulse-chase assay. While the mRNA was unstable in control cells, overexpression of wild-type KSRP only moderately enhanced mRNA decay, suggesting that KSRP is not limiting for AMD in these cells. In contrast, overexpression of KSRPL499A further enhanced (~2-fold) mRNA decay (Figures 8A and 8C). In a similar assay, overexpression of KSRPL499A did not enhance the decay rate of a GB mRNA lacking an ARE (Figure S5). To examine whether KSRPL499A displays a stronger ARE-binding activity, we performed UV crosslinking assays with the ARE of GM-CSF as a probe. The RNA-crosslinked wild-type KSRP and KSRPL499A were immunoprecipitated, and we detected a 2-fold increase in ARE binding by KSRPL499A (Figures 8D and 8E). Analogous UV crosslinking and immunoprecipitation assays showed that KSRPL499A binds to the ARE of TNFα stronger than wild-type KSRP and that neither wild-type nor mutant bind to a non-ARE RNA (Figure S6). These results suggest that the enhancement in AMD by KSRPL499A is due to an increase in its ARE-binding activity.

To test RNA binding in vitro, we compared the binding of wild-type KH1234 and mutant KH1234L499A constructs to a TNFα-derived RNA 25-mer. Data from two equivalent

Table 2. Dissociation Constants for the KH3, KH4, and KH34-RNA Complexes, as Determined by NMR and CD

RNA Oligonucleotides	KH3 (NMR) (μM)	KH3 (CD) (μM)	KH4 (NMR) (μM)	KH4 (CD) (μM)	KH34 (CD) (μM)
UAUUUAUUAUUU	8 ± 2	2.0 ± 0.4	31 ± 3	31 ± 30	0.20 ± 0.04
UAUUUA	125 ± 3		270 ± 30		
UAUUAU	140 ± 20		350 ± 30		

The experimental conditions were 27°C (pH 7.4) for NMR and 5°C (pH 7.4) for CD titrations, respectively.

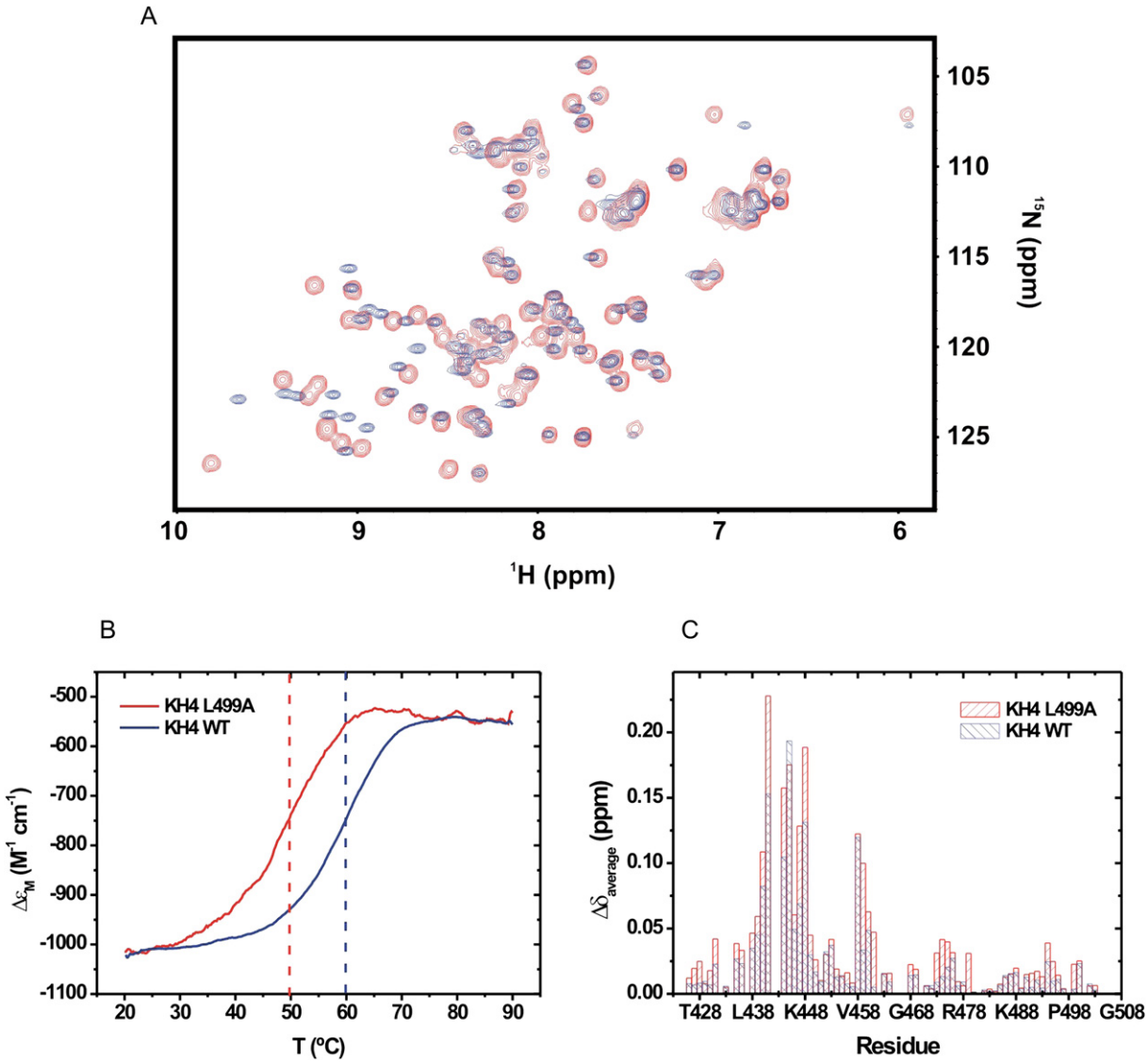

Figure 7. Role of KH4 β_4 in Domain Stability and RNA Binding

(A) Superposition of the ^{15}N-HSQC spectra of the wild-type (blue) and L499A mutant (red) KH4 domain at 27°C and pH 7.4. The domain is stable at 27°C and conserves a KH fold.

(B) CD-monitored thermal unfolding curves of wild-type (blue) and mutant L499A (red) KH4. Vertical lines cross the midpoint of the transition. The mutation lowers the midpoint of the transition by ~10°C.

(C) Comparison of amide chemical-shift changes of KH4 and KH4L499A upon binding to the UAUUUA RNA. Changes at a 1:2 protein/RNA ratio are plotted versus the amino acid sequence for wild-type (blue columns) and mutant L499A (red columns) KH4.

CD titrations returned a slightly higher affinity for the mutant-RNA interaction (K_d = 2 ± 1 nM) than for the wild-type-RNA interaction (K_d = 6 ± 2 nM), confirming that the mutation leads to a limited increase in the RNA-binding capability of the domain. In order to investigate if the observed increase in binding was due to a direct contact of the mutated amino acid/strand with the RNA, we compared the results of NMR titrations of the wild-type KH4 and mutant KH4L499A domains with the UAUUUA RNA. Only small chemical-shift changes are visible for the resonances of β_4 upon RNA binding for both wild-type and mutant (Figure 7C). Titrations with the UAUUUAUUAUUU oligo yielded similar results. These data indicate that it is unlikely that amino acids in strand β_4 contact directly the RNA.

The results of the functional and biophysical assays on the KH4L499A mutant point toward a regulatory role for β_4, where the strand tunes RNA recognition. The importance of this regulatory role could go well beyond a 2-fold increase of activity as we have only weakened the interaction with the protein core, not removed the strand completely.

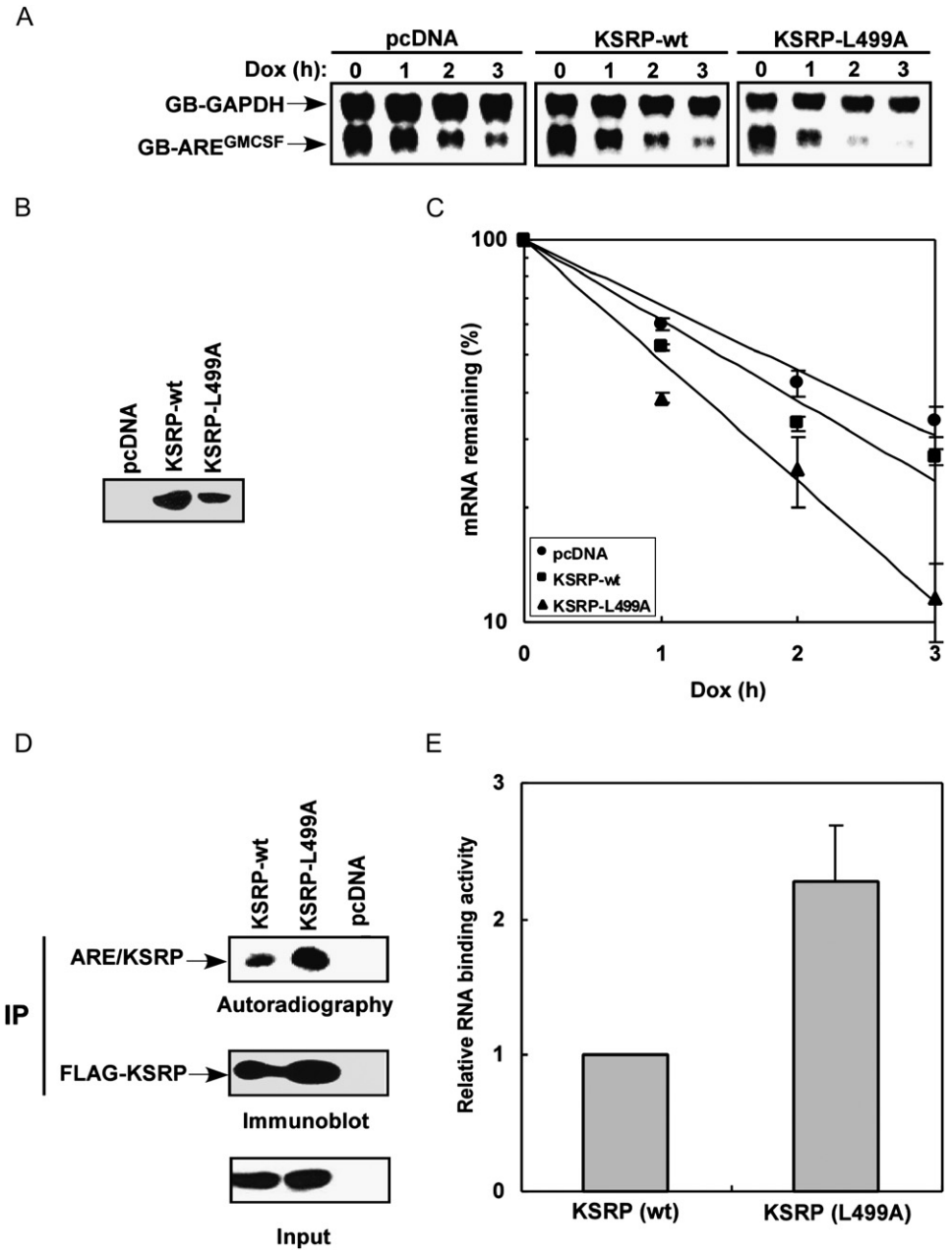

Figure 8. Functional Characterization of KSRPL499A

(A) HT1080-TO cells were transfected with a construct expressing GB-ARE^{GMCSF} mRNA, under the control of a Tet-regulatory promoter, a construct constitutively expressing GB-GAPDH mRNA (serves as a loading control), and constructs expressing either the wild-type FLAG-KSRP or FLAG-KSRPL499A. The decay of GB-ARE^{GMCSF} mRNA was analyzed after the addition of doxycycline by northern blot.

(B) Immunoblot analysis shows expression of transfected proteins with an anti-FLAG antibody.

(C) Signals of GB-ARE^{GMCSF} mRNA in (A) were quantitated by a phosphorimager, normalized to that of GB-GAPDH mRNA, and plotted as mean values ± SDs against time (n = 2).

(D) HT1080-TO cells were transfected with vectors expressing FLAG-KSRP or FLAG-KSRPL499A. Cytoplasmic extracts were prepared, incubated with ^{32}P-labeled ARE^{GMCSF} RNA, and UV crosslinking assays performed. The UV crosslinking reactions were immunoprecipitated with anti-FLAG agarose and the immunoprecipitates analyzed by SDS-PAGE and autoradiography (top panel) or immunoblotting with anti-FLAG (middle panel). Input used for UV crosslinking and immunoprecipitation assays and analyzed by anti-FLAG is also shown (bottom panel).

(E) The levels of KSRP- or KSRPL499A-bound RNA (top panel in [D]) were quantitated by a phosphorimager and normalized by the densitometer-analyzed protein levels (middle panel in [D]). The levels of KSRP-bound RNA after normalization were set as 1. Mean values with standard deviations (SD) are shown (n = 2).

DISCUSSION

The criteria used by KSRP to recognize its RNA targets are unknown, and to date, there are no reports that provide an explanation for its selectivity at the molecular level. In this work, we focus on the features that confer plasticity to the recognition mechanism allowing KSRP to bind heterogeneous sequence targets in different structural environments as well as on the regulation of the recognition mechanism itself.

General Features of KSRP-RNA Recognition

The key domains in the KSRP-RNA interaction, KH3 and KH4, are structurally very similar if we exclude the fourth strand of KH4. Do these domains interact? Interdomain interactions have been described for several RNA-binding proteins and have been shown to be important for RNA recognition. In some cases, such as NusA, the protein uses tightly packed sequential domains to form a continuous RNA-binding surface that recognizes a long RNA sequence (Beuth et al., 2005), while in other cases, (e.g., PTB) it uses strong, pre-existing interdomain contacts to modify the RNA architecture and drive functional recognition (Oberstrass et al., 2005). Contrarily FBP, a sequence-specific DNA-binding protein related to KSRP, uses its KH domains as completely independent binding units (Braddock et al., 2002). The unstructured RNA regions bound by the KSRP KH domains lie within large and structured 3′UTRs, and strong pre-existing interdomain interactions would limit the capability of the protein to adapt to different structural contexts. Three independent pieces of evidence (chemical shift values, stability, and τ_c values) demonstrate the absence of specific interactions between KH3 and KH4 and explain the plasticity shown by the two-domain construct in the recognition of its highly heterogeneous RNA targets. However, this does not exclude the existence of an interaction when the two domains are bound to RNA. Steric hindrance may limit the freedom of the domain to fit some 3′UTR structures, and protein-protein contacts in the large protein-RNA complexes may be important for the regulation of an RNA-driven recognition.

No clear consensus exists on how ARE-BP-RNA interactions are regulated, although it has been shown that the secondary structure of the RNA target is important to the recognition by the ARE-BP AUF1 in vitro (Wilson et al., 2001). KH3 and KH4 can adapt to both different sequences and different structures, and this provides the protein with a flexible recognition unit. In KSRP, the apparent contradiction between the importance of KH4 in ARE recognition and its weak in vitro RNA-binding capability raises the possibility of a regulatory role for this domain.

The analysis of the interaction between KH3 and KH4 and ARE-derived RNA sequences shows that both KH3 and KH4 bind to ARE-derived RNA oligos by using the canonical nucleic-acid-binding surface of the KH domain and that KH3 binds tighter than KH4. Interestingly, we have shown that both KH3 and KH4 bind with similar affinity to RNA oligonucleotides spanning different sections of TNFα ARE; that is, single domains do not have a strong positional preference within the ARE. The RNA-binding properties of KH3, KH4, and the two-domain construct indicate that it is likely that both domains participate in the recognition in vivo, each providing a significant share of the binding affinity.

Regulatory Role of the KH4 Domain

KH4 is a canonical KH domain except for a novel extension in the form of a fourth β strand. This extension is conserved in the KSRP family and is not present in KH1, KH2, or KH3. Insertions of secondary structure elements within the well-conserved topologies of different RNA-binding motifs have been shown to further their molecular recognition abilities. The addition of a helix, the so-called QUA2 element, extends the RNA-binding surface of the KH domain of splicing factor 1 protein (Liu et al., 2001), thereby increasing the specificity of this protein. A similar effect is achieved by a strand intercalating between helix α_2 and strand β_4 of the central RRM-RNA-binding motif of the La protein or by an additional strand at the C terminus of the RRM2 and RRM3 domains of PTB (Alfano et al., 2003; Oberstrass et al., 2005). Ad hoc structural elements can also regulate RNA binding by sequestering the RNA-binding surface (Allain et al., 1996) or by orienting other elements in a position optimal for RNA binding. A helix-positioned C-terminal to the classical dsRBM fold of the yeast protein Rnt1p orients helix1 in the correct position and allows recognition of a tetra-loop structure within the RNA target (Leulliot et al., 2004).

In KH4 of KSRP, the additional β strand does not represent a direct extension of the RNA-binding surface (Figure 5C), and the small size of the chemical-shift changes undergone by β_4 upon RNA binding (both in KH4 and KH34) indicates that direct contact with the RNA is unlikely. The strand does not cover or preclude access to the RNA-binding surface either (Figure 5B) and therefore cannot function in a ''lid''-like manner.

How does β_4 tune the binding to RNA targets? An indirect structural tuning by orienting the elements directly involved in the interaction and/or a change in the dynamics of the RNA-binding surface represents an explanation for the observed increase in mRNA decay. Comparison of NMR data on the wild-type and L499A mutant protein shows chemical-shift changes across the whole β sheet (Figure S4A). Further, relaxation data show a general increase in flexibility in the mutant (Figure S4B). In the third KH domain of Nova-1 protein, the motions of some residues in the RNA-binding groove are affected by protein-protein interactions occurring on the opposite surface of the domain (Ramos et al., 2002); this effect has been proposed to mediate functional RNA binding. It seems possible that KH4 β_4 exerts a regulatory effect by controlling the geometry/dynamics of the RNA-binding groove of the domain. Importantly, the role of β_4 in mRNA decay is likely to be linked to the interaction of KSRP with other functional partners and possibly with the C-terminal region of the protein.

Our study explains that the broad specificity of KSRP-RNA recognition is linked to the weak preference showed by each domain for the ARE targets and to the relation between domains. The role of KH4 in mRNA degradation does not stem from a strong sequence-specific RNA-binding activity but from a more complex regulatory function that is performed in the context of the multidomain protein. This function is likely to be at the core of the plasticity of KSRP, a plasticity that is at the basis of the AMD modulation network.

EXPERIMENTAL PROCEDURES

Cloning, Expression, and Purification of the Protein Constructs and Preparation of the RNA Oligonucleotides

All clones were constructed by PCR from a plasmid containing full-length KSRP (Gherzi et al., 2004). The boundaries of the original KH3, KH4, and KH34 constructs (Figure 1) were as reported (Gherzi et al., 2004). The shorter KH4 clone (ΔKH4) spanned amino acids 423–496. PCR products were ligated into the NcoI and HindIII sites of pETM-30, which codes for a His-GST fusion with a TEV cleavage site N-terminal to the insert. Mutagenesis was performed by using the Quikchange Site-Directed Mutagenesis Kit (Stratagene) according to manufacturer's instructions.

Labeled and unlabeled proteins were expressed in *Escherichia coli* BL21 (DE3) (Invitrogen) as reported (Ramos et al., 2006). The His-GST-fusion protein was initially purified by nickel affinity chromatography according to the manufacturer's instructions. The bulky His-GST fusion tags were then cleaved with TEV protease and removed by using a second nickel affinity step. The constructs were then further purified and buffer exchanged by gel filtration (Superdex 75 16/60 column, Pharmacia). Final buffer was 10 mM Tris (pH 7.4) and 50 mM NaCl, 0.5 mM TCEP. Protein purity (always >95%) was assessed by SDS-PAGE and Coomassie staining. Protein quantification was achieved by a combination of spectrophotometry using predicted extinction coefficients and ninhydrin analysis of protein hydrolysates. All RNA oligonucleotides were chemically synthesized (Curevac).

CD Spectroscopy

All CD spectra were recorded on Jasco J-715 spectropolarimeter (Jasco) equipped with a PTC-348 Peltier temperature-control system. CD intensities are presented as the CD absorption coefficient calculated by using the molar concentration of the proteins. Thermal unfolding of KH3, KH4, and KH34 was monitored between 15°C and 90°C. Temperature was increased at a rate of 1°C per min and unfolding was monitored by recording the signal at 220 nm. Reversibility was assessed by cooling to 15°C at the same rate. Protein concentrations were 1–2 μM in 10 mM Tris-HCl (pH 7.4), 100 mM NaCl, 0.5 mM TCEP. The data were processed and fitted to a two-state model as described in García-Mayoral et al. (2006). The percentages of folded and unfolded protein at different temperatures were calculated from the values of ΔG_T assuming a ΔC_p of 1 kcal/mol K (Masino et al., 2000).

RNA binding was monitored by adding increasing amounts of protein to 1–2 μM RNA oligonucleotides in 10 mM Tris-HCl (pH 7.4), 100 mM NaCl, 0.5 mM TCEP. Temperatures were chosen to optimize the signal change upon protein binding and were 5°C and 20°C for the UAUUUAUUAUUU and the UAUUUAUUAUUUAUUUAUUAUUUAU RNAs, respectively. The integral of the signal between 255 and 265 nm was fitted against the protein concentration with in-house programs as described in Martin et al. (2000), and the values of the K_ds were extracted.

NMR Spectroscopy and Resonance Assignment

The different samples of the KSRP KH3, KH4, and KH34 constructs were prepared in 90% H_2O/10% D_2O solutions of 10 mM Tris-HCl buffer, 50–100 mM NaCl, 1 mM TCEP, 0.02% NaN_3 (pH 7.4) at concentrations in the range 0.5–1 mM. NMR spectra were recorded by using ^{15}N or $^{15}N/^{13}C$-labeled samples at 15°C and 27°C on Varian Inova and Bruker Avance spectrometers operating at 600 and 800 MHz ^1H frequencies. The spectra were processed with the NMRPipe package (Delaglio et al., 1995) and analyzed with Sparky (Goddard and Kneller, 2004).

^1HN, ^{15}N, $^{13}C_\alpha$, $^{13}C_\beta$, and $^{13}C'$ assignments were achieved from standard HNCACB, CBCA(CO)NH, HNCA, HN(CO)CA, and HNCO backbone experiments (Bax and Grzesiek, 1993). Side-chain resonance assignment was obtained from ^{15}N and ^{13}C-edited NOESY-HSQC spectra with 100 ms mixing time (Fesik and Zuiderweg, 1988). The WATERGATE pulse sequence (Piotto et al., 1992) was used for water suppression. $^3J_{HN\text{-}H\alpha}$ scalar couplings were measured from HNHA experiments as described (Vuister and Bax, 1993).

Relaxation Data and Residual Dipolar Couplings

T_1, T_2, and $\{^1H\}$-^{15}N NOE parameters were obtained from standard experiments (Kay et al., 1989) recorded on ^{15}N-labeled samples at 27°C and 600 MHz ^1H frequency and analyzed by using NMRPipe routines (Delaglio et al., 1995). T_1/T_2 of residues in well-defined secondary structure regions was used to estimate the rotational correlation times (τ_c) of the protein constructs with the program TENSOR (Dosset et al., 2000), assuming overall isotropic motion.

To measure residual dipolar couplings (RDCs), ^{15}N-^{13}C samples of protein were prepared in buffer alone (10 mM Tris-HCl, 50 mM NaCl, 1 mM TCEP [pH 7.4]) or binary mixtures of ~5% (v/v) alkyl-poly(ethylene glycol) $C_{12}E_5$ and ~1% (v/v) hexanol in the same buffer, as described in Rückert and Otting (2000), that were magnetically aligned at 600 MHz ^1H frequency. ^{15}N-^1H amide RDCs were measured by using 2D IPAP-HSQC spectra (Ottiger et al., 1998). $^{13}C_\alpha$-$^1H_\alpha$ RDCs were measured in a modified 3D (HA)CA(CO)NH experiment (Tjandra and Bax, 1997) without $^1H_\alpha$ decoupling in the ^{13}C dimension. The dipolar couplings were calculated from the difference in the coupling constants measured in isotropic and nonisotropic conditions.

The magnitude, D_a (axial component), and rhombicity (R) of each alignment tensor were independently calculated in the absence of structural information from the whole-powder pattern distribution of the two sets of measured RDCs, after normalizing $^{13}C_\alpha$-$^1H_\alpha$ dipolar couplings with respect to the ^{15}N-^1H dipolar interaction (Clore et al., 1998).

Structure Calculation and Analysis

Structure calculations were performed with ARIA 1.2 (Linge et al., 2001) by using distance and angle restraints. Experimental distance restraints (Table 1) were obtained from Sparky NOE peak lists integrated with XEASY (Bartels et al., 1995). Dihedral restraints were obtained from experimentally measured scalar couplings (ϕ, KH3 and KH4) (Ye et al., 2001) and from the chemical-shift-based TALOS database (ϕ and φ, KH3 only) (Cornilescu et al., 1999). H-bond constraints were added when unambiguously identified by the structural analysis of the preliminary structures.

Two hundred randomized conformers underwent simulated annealing with a standard CNS protocol as described in de Chiara et al. (2005). The 20 lowest-energy resulting structures were water refined (Linge et al., 2003) in the PARALLHDG 5.3 force field. Structural statistics are reported in Table 1. The quality of each family has been evaluated with PROCHECK_NMR (Laskowski et al., 1996). The structures were displayed and analyzed with MOLMOL (Koradi et al., 1996). The structures of the KSRP KH3 and KH4 domains have been deposited in the PDB with the accession identifiers 2HH3 and 2HH2, respectively. Multiple sequence alignments were done with the CLUSTALX program (Jeanmougin et al., 1998) and searches of closely related proteins based on structural alignments with the DALI database server (http://www.ebi.ac.uk/dali/).

NMR Monitoring of Domain Stability and RNA Binding

The thermal stability of the domains was monitored by recording ^{15}N-HSQC spectra on 600 MHz (KH3 and KH4) and 800 MHz (KH34)

VARIAN-INOVA spectrometers on ~0.3 mM protein samples in 10 mM Tris-HCl buffer, 50 mM NaCl, 1 mM TCEP (pH 7.4). Spectra were recorded at 3°C intervals between 27°C and 69°C. Protein unfolding was fully reversible.

Solutions of 25–75 μM ^{15}N-labeled samples of KH3 and KH4 in 10 mM Tris-HCl buffer, 50 mM NaCl, 1 mM TCEP (pH 7.4) were titrated with (5′-UAUUUA-3′), (5′-UAUUAU-3′), and (5′-UAUUUAUUAUUU-3′) RNA oligonucleotides (Table 2). ^{15}N-HSQC spectra were recorded at each point of the titration at 27°C. Amide chemical-shift changes as a function of protein/RNA ratio were fitted to obtain the K_d values for the complexes with in-house software as described in Martin et al. (2004). Weighted average values of ^{15}N and ^{1}H chemical shift variations have been calculated as follows: $\Delta\delta_{av} = ([\Delta\delta^{1}H]^2 + [\Delta\delta^{15}N]^2/10)^{1/2}$.

Establishment of an HT1080-TO Cell Line and mRNA Decay Analysis

To establish the tetracycline (Tet)-Off (TO) system in HT1080 fibrosarcoma cell line, HT1080 cells were transfected with the pTet-Off plasmid (Clontech) expressing tetracycline-controlled transactivator (tTA) that activates transcription in the absence of doxycycline (Dox). Individual stable clones were selected with G418 and analyzed for the repression of luciferase reporter gene expression under the control of a Tet-regulatory promoter upon Dox addition. A cloned cell line exhibiting about 20-fold repression upon the addition of Dox was chosen for subsequent mRNA decay analysis.

The established HT1080-TO cells were plated onto 6-well plates and transfected with lipofectamine. After transfection, cells were treated with tetracycline (50 ng/ml). To examine mRNA decay, a 16 hr transcriptional pulse was employed, followed by addition of doxycycline (2 μg/ml). Cytoplasmic RNA was isolated at different times. mRNA decay analyzed by northern blot was previously described (Chou et al., 2006; Gherzi et al., 2004).

Supplemental Data

Supplemental Data include the comparison of chemical-shift differences between isolated KH3 and KH4 and the two-domain construct KH34; T_1 and heteronuclear NOE relaxation data for KH3, KH4, and KH34; ^{15}N-HSQC spectra of the ΔKH4 construct at two different temperatures; mapping of chemical-shift perturbations in the KH4L499A mutant compared to KH4 wild-type, T_1, and T_2 relaxation data for the KH4L499A mutant; comparison of non-ARE mRNA decay rates for KSRP wild-type and KSRPL499A mutant; comparison of KSRP wild-type and KSRPL499A mutant binding to ARE and non-ARE containing RNAs; table with alignment tensor parameters and rotational correlation times for isolated KH3 and KH4, and KH3 and KH4 within KH34; table with KH3, KH4, and KH34 relaxation data (T_1, T_2, heteronuclear NOE) with errors. These data are available at http://www.structure.org/cgi/content/full/15/4/485/DC1/.

ACKNOWLEDGMENTS

We would like to thank Dr. T. Frenkiel for its help in NMR spectra recording and Dr. S. Martin for help in the recording and analysis of CD spectra. We would also like to thank Drs. P. Rosenthal and A. Pastore for critical reading of the manuscript. I.D.-M. is supported by European Molecular Biology Organization fellowship number 240-2005.

Received: November 11, 2006
Revised: March 1, 2007
Accepted: March 14, 2007
Published: April 17, 2007

REFERENCES

Alfano, C., Babon, J., Kelly, G., Curry, S., and Conte, M.R. (2003). Resonance assignment and secondary structure of an N-terminal fragment of the human La protein. J. Biomol. NMR *27*, 93–94.

Allain, F.H.T., Gubser, C.C., Howe, P.W.A., Nagai, K., Neuhaus, D., and Varani, G. (1996). Specificity of ribonucleoprotein interaction determined by RNA folding during complex formation. Nature *380*, 646–650.

Audic, Y., and Hartley, R.S. (2004). Post-transcriptional regulation in cancer. Biol. Cell *96*, 479–498.

Baber, J.L., Libutti, D., Levens, D., and Tjandra, N. (1999). High precision solution structure of the C-terminal KH domain of heterogeneous nuclear ribonucleoprotein K, a c-*myc* transcription factor. J. Mol. Biol. *289*, 949–962.

Bakheet, T., Williams, B.R., and Khabar, K.S. (2006). ARED 3.0: the large and diverse AU-rich transcriptome. Nucleic Acids Res. *34*, D111–D114.

Barreau, C., Paillard, L., and Osborne, H.B. (2006). AU-rich elements and associated factors: are there unifying principles? Nucleic Acids Res. *33*, 7138–7150.

Bartels, C., Xia, T.-H., Billeter, M., Güntert, P., and Wüthrich, K. (1995). The program XEASY for computer-supported NMR spectral analysis of biological macromolecules. J. Biomol. NMR *5*, 1–10.

Bax, A., and Grzesiek, S. (1993). Methodological advances in protein NMR. Acc. Chem. Res. *26*, 131–138.

Bernadó, P., Fernandes, M.X., Jacobs, D.M., Fiebig, K., García de la Torre, J., and Pons, M. (2004). Interpretation of NMR relaxation properties of Pin1, a two-domain protein, based on Brownian dynamic simulations. J. Biomol. NMR *29*, 21–35.

Beuth, B., Pennell, S., Arnvig, K.B., Martin, S.R., and Taylor, I.A. (2005). Structure of a *Mycobacterium tuberculosis* NusA-RNA complex. EMBO J. *24*, 3576–3587.

Braddock, D.T., Cai, M.L., Baber, J.L., Huang, Y., and Clore, G.M. (2001). Rapid identification of medium- to large-scale interdomain motion in modular proteins using dipolar couplings. J. Am. Chem. Soc. *123*, 8634–8635.

Braddock, D.T., Louis, J.M., Baber, J.L., Levens, D., and Clore, G.M. (2002). Structure and dynamics of KH domains from FBP bound to single-stranded DNA. Nature *415*, 1051–1056.

Briata, P., Forcales, S.V., Ponassi, M., Corte, G., Chen, C.-Y., Karin, M., Puri, P.L., and Gherzi, R. (2005). p38-dependent phosphorylation of the mRNA decay-promoting factor KSRP controls the stability of select myogenic transcripts. Mol. Cell *20*, 891–903.

Chou, C.F., Mulky, A., Maitra, S., Lin, W.J., Gherzi, R., Kappes, J., and Chen, C.Y. (2006). Tethering KSRP, a decay-promoting AU-rich element-binding protein, to mRNAs elicits mRNA decay. Mol. Cell. Biol. *26*, 3695–3706.

Clore, G.M., Gronenborn, A.M., and Bax, A. (1998). A robust method for determining the magnitude of the fully asymmetric alignment tensor of oriented macromolecules in the absence of structural information. J. Magn. Reson. *133*, 216–221.

Cornilescu, G., Delaglio, F., and Bax, A. (1999). Protein backbone angle restraints from searching a database for chemical shift and sequence homology. J. Biomol. NMR *13*, 289–302.

Delaglio, F., Grzesiek, S., Vuister, G.V., Zhu, G., Pfeifer, J., and Bax, A. (1995). NMRPipe: a multidimensional spectral processing system based on UNIX pipes. J. Biomol. NMR *6*, 277–293.

de Chiara, C., Menon, R.P., Adinolfi, S., de Boer, J., Ktistaki, E., Kelly, G., Calder, L., Kioussis, D., and Pastore, A. (2005). The AXH domain adopts alternative folds: the solution structure of HBP1 AXH. Structure *13*, 743–753.

Dosset, P., Hus, J.C., Blackledge, M., and Marion, D. (2000). Efficient analysis of macromolecular rotational diffusion from heteronuclear relaxation data. J. Biomol. NMR *16*, 23–28.

Fesik, S.W., and Zuiderweg, E.R.P. (1988). Heteronuclear 3-dimensional NMR spectroscopy. A strategy for the simplification of homonuclear two-dimensional NMR spectra. J. Magn. Reson. *78*, 588–593.

García-Mayoral, M.F., Martínez del Pozo, A., Campos-Olivas, R., Gavilanes, J.G., Santoro, J., Rico, M., Laurents, D.V., and Bruix, M. (2006). pH-dependent conformational stability of the ribotoxin α-sarcin and four active site charge substitution variants. Biochemistry *45*, 13708–13718.

Gherzi, R., Lee, K.-Y., Briata, P., Wegmüller, D., Moroni, C., Karin, M., and Chen, C.-Y. (2004). A KH domain RNA binding protein, KSRP, promotes ARE-directed mRNA turnover by recruiting the degradation machinery. Mol. Cell *14*, 571–583.

Gherzi, R., Trabucchi, M., Ponassi, M., Ruggiero, T., Corte, G., Moroni, C., Chen, C.-Y., Khabar, K.S., Andersen, J.S., and Briata, P. (2006). The RNA-binding protein KSRP promotes decay of β-catenin mRNA and is inactivated by PI3K-AKT signaling. PLoS Biol. *5*, e5. 10.1371/journal.pbio.0050005.

Goddard, T.D., and Kneller, D.G. (2004). Sparky (computer program) (San Francisco: University of California).

Holm, L., and Sander, C. (1993). Protein structure comparison by alignment of distance matrices. J. Mol. Biol. *233*, 123–138.

Hudson, B.P., Martínez-Yamout, M.A., Dyson, H.J., and Wright, P.E. (2004). Recognition of the mRNA AU-rich element by the zinc finger domain of TIS11d. Nat. Struct. Mol. Biol. *11*, 257–264.

Jeanmougin, F., Thompson, J.D., Gouy, M., Higgins, D.G., and Gibson, T.J. (1998). Multiple sequence alignment with Clustal X. Trends Biochem. Sci. *23*, 403–405.

Kay, L.E., Torchia, D.A., and Bax, A. (1989). Backbone dynamics of proteins as studied by ^{15}N inverse detected heteronuclear NMR spectroscopy: application to staphylococcal nuclease. Biochemistry *28*, 8972–8979.

Kontoyannis, D., Pasparakis, M., Pizarro, T.T., Cominelli, F., and Kollias, G. (1999). Impaired on/off regulation of TNF biosynthesis in mice lacking TNF AU-rich elements: implications for joint and gut-associated immunopathologies. Immunity *10*, 387–398.

Koradi, R., Billeter, M., and Wüthrich, K. (1996). MOLMOL: a program for display and analysis of macromolecular structures. J. Mol. Graph. *14*, 51–55, 29–32.

Laskowski, R.A., Rullman, J.A., MacArthur, M.W., Kaptein, R., and Thorton, J.M. (1996). AQUA and PROCHECK-NMR: programs for checking the quality of protein structures solved by NMR. J. Biomol. NMR *8*, 477–486.

Leulliot, N., Quevillon-Cheruel, S., Graille, M., van Tilbeurgh, H., Leeper, T.C., Godin, K.S., Edwards, T.E., Sigurdsson, S.T.L., Rozenkrants, N., Nagel, R.J., et al. (2004). A new alpha-helical extension promotes RNA binding by the dsRBD of Rnt1p RNAse III. EMBO J. *23*, 2468–2477.

Lewis, H.A., Musunuru, K., Jensen, K.B., Edo, C., Chen, H., Darnell, R.B., and Burley, S.K. (2000). Sequence-specific RNA binding by a Nova KH domain: implications for paraneoplastic disease and the fragile X syndrome. Cell *100*, 323–332.

Linge, J.P., O'Donoghue, S.I., and Nilges, M. (2001). Automated assignment of ambiguous nuclear overhauser effects with ARIA. Methods Enzymol. *339*, 71–90.

Linge, J.P., Williams, M.A., Spronk, C.A., Bonvin, A.M., and Nilges, M. (2003). Refinement of protein structures in explicit solvent. Proteins *50*, 496–506.

Liu, Z.H., Luyten, I., Bottomley, M.J., Messias, A.C., Houngninou-Molango, S., Sprangers, R., Zanier, K., Kramer, A., and Sattler, M. (2001). Structural basis for recognition of the intron branch site RNA by splicing factor 1. Science *294*, 1098–1102.

Martin, S.R., Masino, L., and Bayley, P.M. (2000). Enhancement by Mg^{2+} of domain specificity in Ca^{2+}-dependent interactions of calmodulin with target sequences. Protein Sci. *9*, 2477–2488.

Martin, S.R., Biekofsky, R.R., Skinner, M.A., Guerrini, R., Salvadori, S., Feeney, J., and Bayley, P.M. (2004). Interaction of calmodulin with the phosphofructokinase target sequence. FEBS Lett. *577*, 284–288.

Masino, L., Martin, S.R., and Bayley, P.M. (2000). Ligand binding and thermodynamic stability of a multidomain protein, calmodulin. Protein Sci. *9*, 1519–1529.

Musco, G., Kharrat, A., Stier, G., Fraternali, F., Gibson, T.J., Nilges, M., and Pastore, A. (1997). The solution structure of the first KH domain of FMR1, the protein responsible for the fragile X syndrome. Nat. Struct. Mol. Biol. *4*, 712–716.

Musunuru, K., and Darnell, R.B. (2004). Determination and augmentation of RNA sequence specificity of the Nova K-homology domains. Nucleic Acids Res. *32*, 4852–4861.

Oberstrass, F.C., Auweter, S.D., Erat, M., Hargous, Y., Henning, A., Wenter, P., Reymond, L., Amir-Ahmady, B., Pitsch, S., Black, D.L., et al. (2005). Structure of PTB bound to RNA: specific binding and implications for splicing regulation. Science *309*, 2054–2057.

Ottiger, M., Delaglio, F., and Bax, A. (1998). Measurement of J and dipolar couplings from simplified two-dimensional NMR spectra. J. Magn. Reson. *131*, 373–378.

Piotto, M., Saudek, V., and Sklenar, V. (1992). Gradient-tailored excitation for single-quantum NMR spectroscopy of aqueous solutions. J. Biomol. NMR *2*, 661–665.

Ramos, A., Hollingworth, D., Major, S.A., Adinolfi, S., Kelly, G., Muskett, F.W., and Pastore, A. (2002). Role of dimerization in KH/RNA complexes: the example of Nova KH3. Biochemistry *41*, 4193–4201.

Ramos, A., Hollingworth, D., Adinolfi, S., Castets, M., Kelly, G., Frenkiel, T.A., Bardoni, B., and Pastore, A. (2006). The structure of the N-terminal domain of the fragile X mental retardation protein: a platform for protein-protein interaction. Structure *14*, 21–31.

Rückert, M., and Otting, G. (2000). Alignment of biological macromolecules in novel nonionic liquid crystalline media for NMR experiments. J. Am. Chem. Soc. *122*, 7793–7797.

Tjandra, N., and Bax, A. (1997). Large variations in ^{13}Cα chemical shift anisotropy in proteins correlate with secondary structure. J. Am. Chem. Soc. *119*, 9576–9577.

Vuister, G.V., and Bax, A. (1993). Quantitative J correlation: a new approach for measuring homonuclear three-bond $J(H^{N}H^{\alpha})$ coupling constants in ^{15}N-enriched proteins. J. Am. Chem. Soc. *115*, 7772–7777.

Wang, X., and Tanaka Hall, T.M. (2001). Structural basis for recognition of AU-rich element RNA by the HuD protein. Nat. Struct. Biol. *8*, 141–145.

Wilson, G.M., Sutphen, K., Chuang, K., and Brewer, G. (2001). Folding of A+U-rich RNA elements modulates AUF1 binding. Potential roles in regulation of mRNA turnover. J. Biol. Chem. *276*, 8695–8704.

Ye, J.Q., Mayer, K.L., Mayer, M.R., and Stone, M.J. (2001). NMR solution structure and backbone dynamics of the CC chemokine eotaxin-3. Biochemistry *40*, 7820–7831.

Accession Numbers

The structures of the KSRP KH3 and KH4 domains have been deposited in the PDB with the accession identifiers 2HH3 and 2HH2, respectively.

